

Current Biology

Striatal neurons expressing dopamine D₁ receptor promote wakefulness in mice

Highlights

- Striatal D₁R neurons are wake active and wake promoting
- Activities of striatal D₁R neurons are highly synchronized with PFC and MD neurons
- Striatal D₁R neurons control wakefulness via striatum → EP and striatum → SNr pathways

Authors

Hui Dong, Ze-Ka Chen, Han Guo, Xiang-Shan Yuan, Cheng-Wei Liu, Wei-Min Qu, Zhi-Li Huang

Correspondence

quweimin@fudan.edu.cn (W.-M.Q.),
huangzl@fudan.edu.cn (Z.-L.H.)

In brief

Dong et al. reveal that optogenetic activation of striatal D₁R neurons promotes wakefulness in mice. Conversely, chemogenetic inhibition of D₁R neurons attenuates wakefulness. The activity of D₁R neurons is the highest during wakefulness and is highly synchronized with and regulated by afferent corticostriatal and thalamostriatal neurons.

Article

Striatal neurons expressing dopamine D₁ receptor promote wakefulness in mice

Hui Dong,^{1,2} Ze-Ka Chen,^{1,2} Han Guo,^{1,2} Xiang-Shan Yuan,^{1,2} Cheng-Wei Liu,¹ Wei-Min Qu,^{1,*} and Zhi-Li Huang^{1,3,*}

¹Department of Pharmacology, School of Basic Medical Sciences, State Key Laboratory of Medical Neurobiology and MOE Frontiers Center for Brain Science, Institutes of Brain Science, Fudan University, Shanghai 200032, China

²These authors contributed equally

³Lead contact

*Correspondence: quweimin@fudan.edu.cn (W.-M.Q.), huangzl@fudan.edu.cn (Z.-L.H.)

<https://doi.org/10.1016/j.cub.2021.12.026>

SUMMARY

Patients with Parkinson's disease (PD) suffer from severe sleep disorders. Pathophysiology of the basal ganglia (BG) underlies PD, and the dorsal striatum represents the major input pathway of the BG. However, the roles and mechanisms of the dorsal striatum in controlling sleep-wake cycles remain unknown. To demonstrate the contribution of dopamine D₁ receptor (D₁R)-positive neurons within the dorsal striatum in promoting wakefulness, we combined optogenetic manipulations and fiber photometry with electroencephalography/electromyography recording in D₁R-Cre mice. As a result, optogenetic activation of striatal D₁R neurons induced immediate transitions from non-rapid eye movement (NREM) sleep to wakefulness, whereas inhibition of striatal D₁R neurons attenuated wakefulness by chemogenetics. Multi-channel fiber photometry recordings revealed that the activity of striatal D₁R neurons synchronized with that of BG upstreams, namely the prefrontal cortex and mediodorsal thalamus, in terms of immediate increase in activity during NREM-to-wake transitions and rapid decrease during wake-to-NREM transitions. Further optogenetic manipulations revealed a prominent contribution of striatal D₁R neurons in control of wakefulness by upstream, corticostriatal, thalamostriatal, and nigrostriatal projections and via downstream, striato-entopeduncular, or striatonigral pathways. Taken together, our findings revealed a circuit regulating wakefulness through striatal D₁R neurons. Striatal D₁R neurons play an important role in controlling wakefulness by integrating the corticostriatal, thalamostriatal, and nigrostriatal projections and innervation of striato-entopeduncular or striatonigral pathways.

INTRODUCTION

Patients with Parkinson's disease (PD) suffer from severe sleep disorders, including excessive daytime sleepiness (EDS), insomnia, and rapid eye movement (REM) sleep behavior disorder.¹ EDS affects more than 50% of patients with PD.² PD is attributed to a dysfunction of the dorsal striatum (caudate and putamen [CPU]), which represents the primary input pathway of the basal ganglion. In healthy individuals, regional cerebral blood flow of the striatum—as measured via H₂¹⁵O positron emission tomography (PET)—is decreased during non-REM (NREM) sleep compared with that during wakefulness,^{3–6} suggesting that the dorsal striatum may be implicated in the regulation of wakefulness.

Post-mortem brain tissues from PD patients have been shown to have higher levels of dopamine D₁ receptors (D₁Rs) (identified via specific [3H]-SCH23390 binding) in the dorsal striatum,⁷ which is likely due to the known decrease in striatal dopaminergic transmission in PD brains. Additionally, the selective D₁R agonist, SKF38393, has been shown to efficiently alleviate EDS in Parkinsonian macaque

monkeys.⁸ Moreover, systemic administration of selective D₁R agonists has been shown to induce behavioral arousal in rabbits^{9,10} and rats,¹¹ whereas selective D₁R antagonism has been demonstrated to induce sedation and slow wave sleep in rats.¹² Based on these lines of evidence, we hypothesized that striatal D₁R-expressing neurons may contribute to wakefulness.

Herein, we combined cell-type-specific optogenetic manipulations and fiber photometry with electroencephalography (EEG)/electromyography (EMG) in mice. We found that optogenetic activation of striatal D₁R neurons induced an immediate transition from NREM sleep to wakefulness. Additionally, fiber photometry revealed that striatal D₁R neurons were active during wakefulness and became silent during sleep, and these state-dependent patterns were synchronized with and regulated by those regions providing afferent inputs to striatal D₁R neurons. Furthermore, optogenetic activation of either afferent or efferent pathways of striatal D₁R neurons produced a rapid transition from sleep to arousal. Taken together, our results reveal that striatal D₁R neurons control neural circuits for wakefulness in mice.

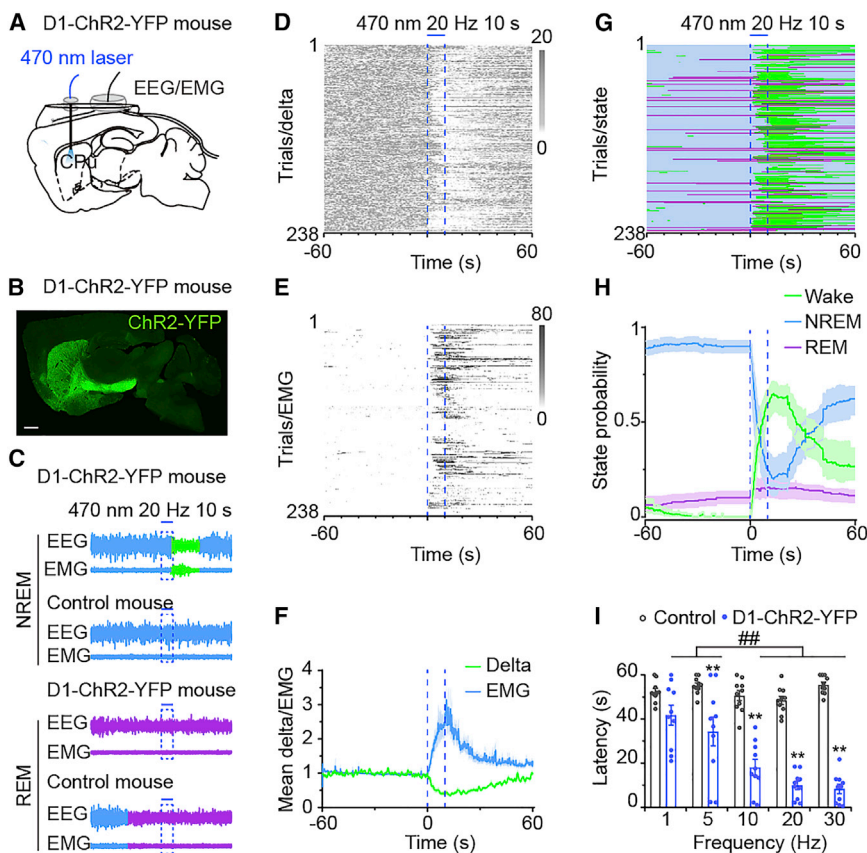


Figure 1. Optogenetic activation of striatal D₁R neurons induces wakefulness

(A) Schematic of laser application and EEG/EMG polysomnographic recordings.

(B) The expression of ChR2-YFP in the dorsal striatum of a D1-ChR2-YFP mouse.

(C) Typical trials with EEG and EMG traces showing an immediate transition from NREM sleep to wakefulness after acute optogenetic stimulation (20 Hz, 5-ms pulse duration, total 10 s) of striatal D₁R neurons in a D1-ChR2-YFP mouse but not in a control mouse. However, stimulation of striatal D₁R neurons did not induce wakefulness from REM sleep. Blue, magenta, and green traces represent NREM sleep, REM sleep and wakefulness, respectively.

(D and E) Delta power of EEGs (D) and RMS of EMGs (E) in all trials from 10 D1-ChR2-YFP mice. (F) The mean delta power of EEGs (green line) and RMS of EMGs (blue line) before, during, and after laser stimulation of striatal D₁R neurons.

(G) Brain states in all trials from 10 D1-ChR2-YFP mice sorted by the order of laser stimulation. Blue, green, and magenta indicate NREM sleep, wakefulness, and REM sleep, respectively.

(H) The probabilities of wake, NREM, or REM states before, during, and after laser stimulation of striatal D₁R neurons.

(I) The latency of transitions from NREM sleep to wakefulness induced by blue-light photostimulation at different frequencies (1–30 Hz) in D1-ChR2-YFP mice or control mice (n = 10 mice per group, two-way ANOVA between frequency and mouse type, $F_{4,72} = 16.017$, $F_{1,18} = 125.46$, $p < 0.001$; compared different frequencies followed by Tukey's multiple test $##p < 0.01$, compared the same frequency followed by Bonferroni's multiple test $**p < 0.01$).

RESULTS

Optogenetic activation of striatal D₁R neurons induces an immediate transition from NREM sleep to wakefulness

To investigate the contribution of striatal D₁R neurons in the control of sleep-wake states, an optogenetic approach was employed in D1-ChR2-YFP mice, which were generated from a Cre-dependent channelrhodopsin (ChR2) mouse line (Ai32)¹³ crossed with a dopamine receptor *Drd1a*-Cre (D₁R-Cre) mouse line.¹⁴ For *in vivo* laser stimulation and sleep-wake recordings, we simultaneously implanted EEG/EMG electrodes and bilateral optical fiber cannulae (Figure 1A). The specific expression of ChR2-YFP in D₁R neurons was verified by yellow fluorescent labeling of striatonigral projections (Figure 1B). To explore the effect of optogenetic activation of striatal D₁R neurons on sleep-wake transitions, we applied 5 ms of blue-light (470 nm) photostimulation at 1–30 Hz for 10 s in D1-ChR2-YFP mice and calculated the delta power of EEGs, the root mean square (RMS) of EMGs, and brain states at both 1 min prior to and subsequent to laser onset. A typical example shows that optical stimulation during NREM sleep induced an immediate transition from NREM sleep to wakefulness in a D1-ChR2-YFP mouse (Figure 1C, upper), as revealed by rapid changes in cortical delta activity and muscle tone compared with these parameters in a

control mouse (Figure 1C). The delta power of EEGs (0.5–4 Hz; Figure 1D), RMS of EMGs (Figure 1E), and brain states (Figure 1G) were aligned for all trials from 10 mice that received laser administration (20 Hz). Photostimulation of striatal D₁R neurons decreased the delta power of the EEG and increased the RMS of the EMG (Figures 1D–1F). The probability of wakefulness increased rapidly at the expense of NREM sleep within 60 s of laser onset (Figure 1H). The latency from NREM sleep to wakefulness was shortened in a stimulation-frequency-dependent manner (Figure 1I; $F_{4,72} = 16.017$, $p = 2.008 \times 10^{-9}$). Photostimulation at 1, 5, 10, 20, or 30 Hz for 10 s in D1-ChR2-YFP mice shortened the latency from NREM sleep to wakefulness by 20.3%, 37.7%, 64.2%, 79.4%, or 84.9%, respectively, compared with that in control mice. Notably, the brain state response was selective for NREM sleep state, as activation of striatal D₁R neurons during REM sleep had no effect (Figure 1C; control group, latency 49.24 ± 3.08 ; D1-ChR2 group, 48.04 ± 5.35 , $t = 0.194$, $p = 0.849$). Taken together, photostimulation of striatal D₁R neurons induced an immediate transition from NREM sleep to wakefulness.

Striatal D₁R neurons are active during spontaneous wakefulness and respond to external stimuli

To assess the population activity of striatal D₁R neurons across spontaneous sleep-wake states in freely moving mice, we

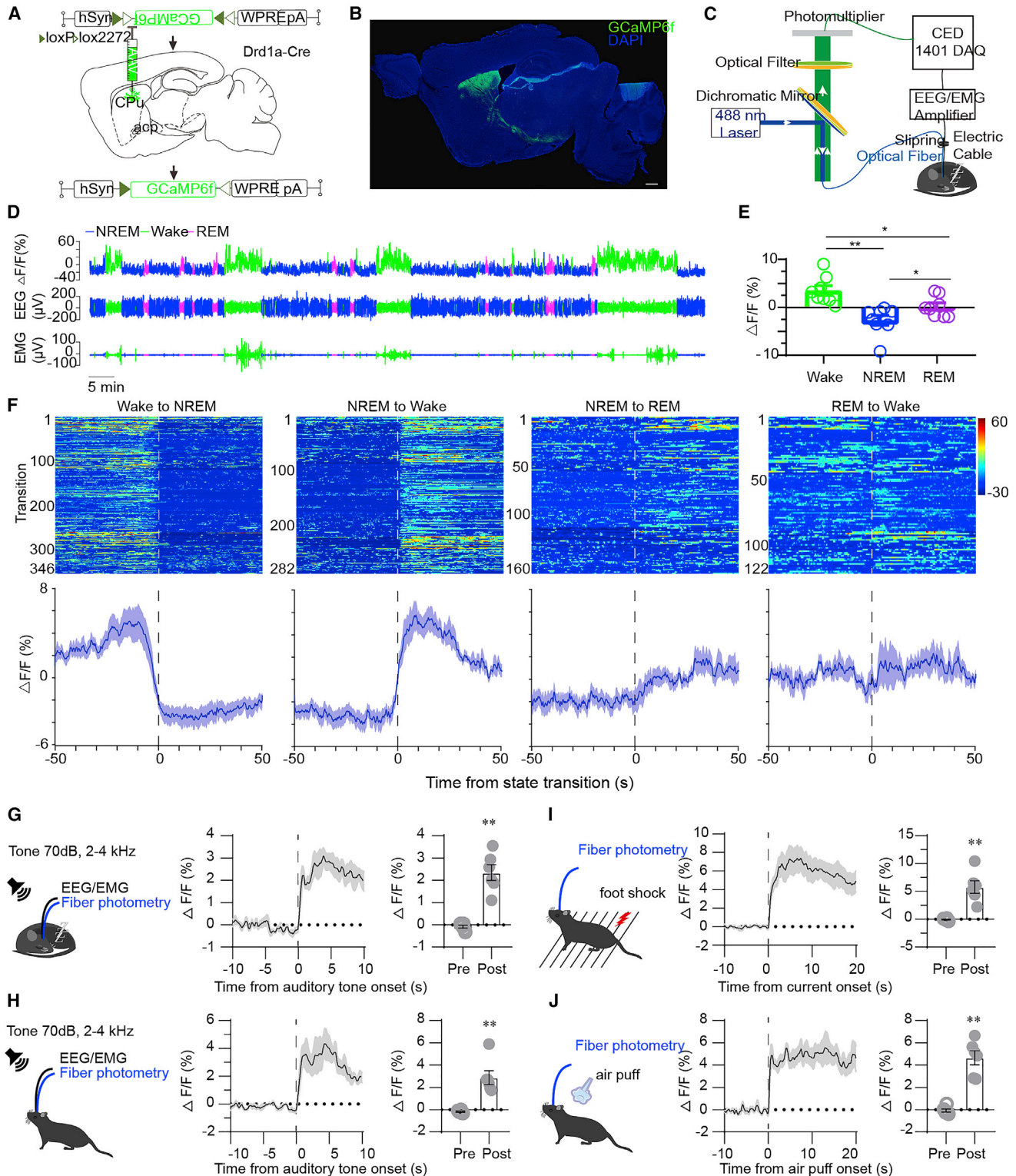


Figure 2. Population activity of striatal D₁R neurons across spontaneous sleep-wake states and in response to salient stimuli

(A) Schematic showing injection of Cre-inducible AAVs expressing GCaMP6f into the dorsal striatum of *Drd1a-Cre* mice.

(B) Image showing expression of GCaMP6f in the dorsal striatum.

(C) Schematic showing the setup of fiber photometry for assessing neuronal population activity with simultaneous polysomnographic recordings.

(D) Representative fluorescent signals and EEG/EMG traces across spontaneous sleep-wake states. Blue indicates NREM sleep, green indicates wakefulness, and magenta indicates REM sleep.

(legend continued on next page)

applied fiber photometry to measure Ca²⁺-dependent fluorescence of GCaMP6f, a genetically encoded calcium indicator,^{15,16} in populations of neurons. A Cre-dependent adeno-associated virus (AAV) encoding GCaMP6f (AAV-hsyn-DIO-GCaMP6f) was injected into the dorsal striatum of *Drd1a*-Cre mice (Figure 2A). GCaMP6f-positive cell bodies were observed in the dorsal striatum (Figure 2B). Calcium and EEG/EMG signals were collected from freely moving mice that were each chronically implanted with a fiber optic probe for subsequent delivery of excitation light and collection of GCaMP6f fluorescent emission, as well as EEG/EMG electrodes for simultaneous polysomnographic recordings (Figure 2C). Striatal D₁R neurons showed higher calcium fluorescence during wakefulness than during REM or NREM sleep (Figure 2D). The GCaMP6f signal of striatal D₁R neurons was significantly higher during wakefulness (3.6% ± 1.0%) than during either REM (0.1% ± 0.8%) or NREM sleep (−2.7% ± 1.0%; Figure 2E; $F_{2,21} = 10.98$, $p = 0.0005$). Notably, striatal D₁R neurons began to increase their activities before NREM-to-wake transitions and decreased their activities before wake-to-NREM transitions (Figure 2F). In contrast, there was no significant difference in the GCaMP6f signals of striatal D₁R neurons during transitions from NREM to REM sleep or from REM sleep to wakefulness (Figure 2F). These findings demonstrated that striatal D₁R neurons increased their activities specifically during the transition from NREM sleep to wakefulness and were most active during spontaneous wakefulness.

To investigate the response dynamics of striatal D₁R neurons to external arousal-provoking stimuli, we recorded the calcium fluorescence of striatal D₁R neurons in mice exposed to diverse salient stimuli. Auditory tone (70 dB, 2–4 kHz frequency, 5-s duration) stimuli were introduced during NREM sleep (Figure 2G) or wakefulness (Figure 2H). When the tone stimulus was given during NREM sleep, the activities of striatal D₁R neurons were immediately increased (Figure 2G; $t_5 = 6.12$, $p = 0.0017$), and mice immediately switched from NREM sleep to wake (Figures S2A and S2B). Striatal D₁R neurons further increased their activities after this tone was delivered during wakefulness (Figure 2H; $t_5 = 4.87$, $p = 0.0046$). Striatal D₁R neurons also showed activation upon delivery of unexpected electric foot shocks (Figure 2I; $t_5 = 5.38$, $p = 0.0030$) or air puffs (Figure 2J; $t_5 = 8.33$, $p = 0.00041$). These findings demonstrate that striatal D₁R neurons are activated not only during spontaneous wakefulness but also in response to arousal-provoking stimuli.

Striatal D₁R neurons are highly synchronized with and regulated by afferent PFC and MD neurons in their activities across spontaneous sleep-wake cycles

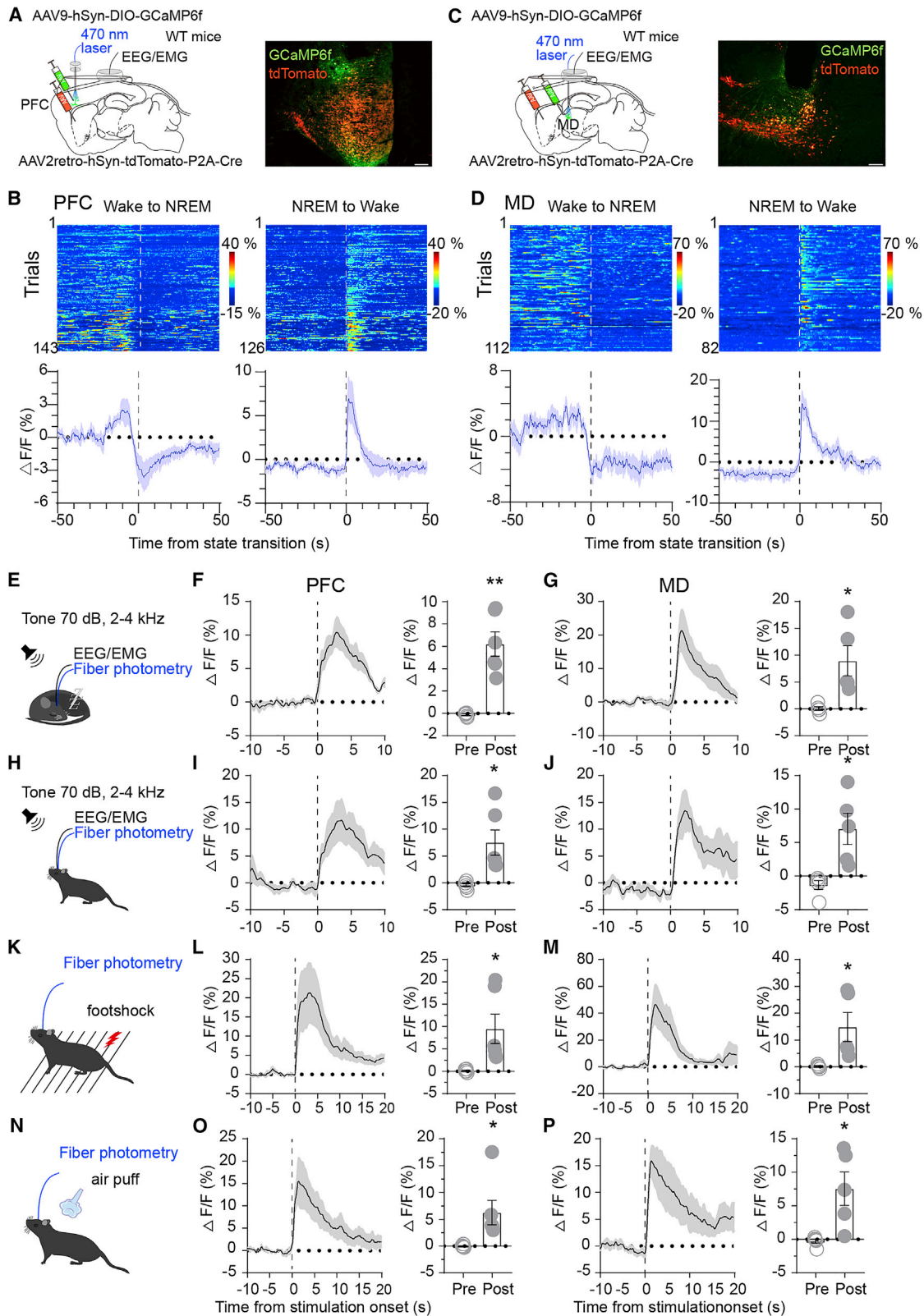
The dorsal striatum receives dopaminergic inputs from the substantia nigra pars compacta (SNc) and the majority of its

glutamatergic inputs from the cerebral cortex and thalamus, whereas GABAergic inputs to the dorsal striatum have rarely been documented. An *in vitro* study demonstrated that medium spiny neurons (MSNs) exhibit negative resting membrane potentials and low firing rates,¹⁷ suggesting that the activity of MSNs may be dominated by their afferent inputs. Therefore, we examined whether regions providing afferent inputs to the dorsal striatum are also implicated in sleep-wake transitions. An AAV encoding GCaMP6f under the control of a Ca²⁺/calmodulin-dependent protein kinase II (CaMKII) promoter, which has been reported to be expressed in glutamatergic neurons in the cortex and thalamus,¹⁸ was injected into the prefrontal cortex (PFC) or mediodorsal thalamus (MD). Additionally, an AAV encoding GCaMP6f in a Cre-inducible manner was injected into the SNc of tyrosine hydroxylase (TH)-Cre mice (Figures S1A, S1C, and S1E). Similar to the activity of striatal D₁R neurons, PFC and MD neurons showed higher calcium fluorescence during wakefulness than during NREM sleep. Both glutamatergic PFC/MD and dopaminergic SNc neurons increased their activities following NREM-to-wake transitions and decreased their activities following wake-to-NREM transitions (Figures S1B, S1D, and S1F). To specifically target the neurons that innervate the dorsal striatum, we applied a viral-based retrograde-labeling approach to record the activities of corticostriatal and thalamostriatal neurons across sleep-wake transitions. We injected the retrograde viral vector, AAV2-retro-hSyn-tdTomato-P2A-Cre, into the dorsal striatum and a Cre-dependent GCaMP6f virus (AAV9-hSyn-DIO-GCaMP6f) into either the PFC or MD (Figures 3A and 3C). Both corticostriatal and thalamostriatal neurons increased their activity during transitions from NREM-to-wake and decreased their activity during wake-to-NREM transitions (Figures 3B and 3D). Interestingly, the Figures 3B and 3D heatmap and averaged traces show that the population neuronal activity of projection-specific PFC-striatum or MD-striatum neurons fell more faster than PFC or MD neurons (Figures 4C and S1). Previous single-cell RNA sequencing and circuit tracing studies report that the PFC and MD neurons have many cell types, and innervate many downstream nuclei.^{19–21} Therefore, the difference in falling rate may be attributed to the population type recorded in projection-specific PFC striatum and MD striatum (Figure 3), which is one of the subtypes of PFC and MD neurons. Furthermore, the activity of corticostriatal and thalamostriatal neurons was also enhanced after application of auditory tone during sleep (Figures 3E–3G; PFC, $t_5 = 5.589$, $p = 0.00253$; MD, $t_4 = 2.975$, $p = 0.0409$) or wakefulness (Figures 3H–3J; PFC, $t_5 = 3.392$, $p = 0.0194$; MD, $t_4 = 4.292$, $p = 0.0127$), or upon delivery of unexpected electric foot shocks (Figures 3K–3M; PFC, $t_5 = 2.949$, $p = 0.0319$; MD, $t_4 = 2.802$, $p = 0.0487$) or air puffs (Figures 3N–3P; PFC, $t_5 = 2.746$, $p = 0.0405$; MD, $t_4 = 2.849$, $p = 0.0464$). These results suggest that the activities of striatal

(E) Mean fluorescence during wakefulness, NREM sleep, and REM sleep ($n = 8$ mice, one-way ANOVA between each state, $F_{2,21} = 10.98$, $p = 0.0005$, followed by Holm-Sidak's multiple comparisons test).

(F) Population activity of striatal D₁R neurons across state transitions. Top: individual transitions with color-coded fluorescent intensities. Bottom: average responses from all the transitions expressed as mean (blue) ± SEM (shaded).

(G–J) Population activity of striatal D₁R neurons in response to acute auditory tones during sleep (G) or wakefulness (H), as well as after foot shocks (I) or air puffs (J). Left: schematic showing application of acute auditory tones, foot shocks, and air puffs. Middle: the time course of the calcium signals of striatal D₁R neurons in response to stimuli. Right: average fluorescence before and after onset of the auditory tone (G, sleep: $t_5 = 6.12$, $p = 0.0017$; H, wake: $t_5 = 4.87$, $p = 0.0046$), foot shock (I, $t_5 = 5.38$, $p = 0.0030$), and air puff (J, $t_5 = 8.33$, $p = 0.00041$).



(legend on next page)

D₁R neurons were affected by their afferent excitatory inputs from the PFC and MD.

To further clarify this phenomenon, we applied multichannel fiber photometry for simultaneous recordings of population activities of PFC, MD, and striatal D₁R neurons. A Cre-independent AAV encoding GCaMP6f driven by the CaMKII promoter was injected into either the PFC or MD, and a Cre-dependent AAV encoding GCaMP6f was simultaneously injected into the dorsal striatum of *Drd1a*-Cre mice. Fiber optic probes were implanted in apposition to these corresponding neuronal populations (Figure 4A). Figure 4B showed that the activities of striatal D₁R neurons, PFC neurons, and MD neurons were simultaneously increased during wakefulness and were decreased during NREM sleep (Figure 4B). Pearson's correlation analysis among these brain regions showed that their neural activities were highly synchronized (D₁R-PFC, $r = 0.6959$; D₁R-MD, $r = 0.3481$, $p < 0.05$). Corticostriatal neurons, thalamostriatal neurons, and striatal D₁R neurons simultaneously increased their activities during NREM-to-wake transitions (Figure 4C) and decreased their activities during wake-to-NREM transitions (Figure 4D).

In addition, to further test whether striatal D₁R neurons activities synchronize with their upstream, dual-color multichannel fiber recording was employed. First, we injected AAV-hSyn-DIO-RCaMP into the striatum and AAV-CaMKII-GCaMP6f into the PFC and MD of *Drd1a*-Cre mice (Figures S4A and S4B). For fiber photometry recording, the tips of fiber optic cannulas were inserted upon the virus injection sites. The 580-nm LED and 488-nm laser were employed to record the signals of RCaMP and GCaMP6f, respectively. Consistent with single-color multichannel fiber recording results, typical traces show that the RCaMP signals of striatal D₁R neurons and GCaMP6f signals of PFC neurons and MD neurons were simultaneously increased during wakefulness and were decreased during NREM sleep (Figures S4C–S4E). Correlation analysis among these brain regions showed that their neural activities were highly synchronized (D₁R-PFC, $r = 0.5833$; D₁R-MD, $r = 0.3667$, $p < 0.05$).

To test the effects on brain states and striatal D₁R neuronal activity after inhibition of the PFC and MD neurons, a chemogenetics approach combined with fiber photometry was employed. AAV-CaMKII α -hM4Di-mCherry was injected into the PFC or MD; meanwhile, AAV-hSyn-DIO-GCaMP6f was injected into the dorsal striatum of *Drd1a*-Cre mice (Figures S5A, S5B, S5E, and S5F). Three weeks after surgery, we found that inhibition of PFC CaMKII neurons by CNO administration (3 mg/kg) resulted in wakefulness decrease as well as NREM sleep increase (Figure S5C), and simultaneously, the peak and frequency of calcium

signals in striatal D₁R neurons was decreased (Figure S5D). We also found that inhibition of MD CaMKII neurons by CNO administration (3 mg/kg) decreased wakefulness significantly (Figure S5G). The peak and frequency of fluorescence signal (mean \pm SEM) in *Drd1a*-Cre mice decreased significantly by CNO administration in the active period (Figure S5H).

These findings show that the calcium activities of striatal D₁R neurons, PFC neurons, and MD neurons are highly synchronized with fluctuations during sleep and wake transitions and that the striatal D₁R neural activity is regulated by the inputs from PFC and MD neurons.

Responses of striatal D₁R neurons, PFC neurons, and MD neurons to external auditory stimuli

We next examined whether the activities of striatal D₁R neurons also correlated with those of their afferent inputs when mice were exposed to salient stimuli. An auditory tone stimulus was introduced during either NREM sleep or wakefulness (Figures S3A and S3C). Under NREM sleep conditions, the activities of striatal D₁R neurons and their afferent inputs in the PFC and MD were simultaneously increased after the onset of the tone stimulus (Figure S3B). The activities of striatal D₁R neurons and their afferent inputs were further increased after the tone was administered during wakefulness (Figure S3D). These findings demonstrated that the activities of striatal D₁R neurons were synchronized with those of their afferent corticostriatal and thalamostriatal neurons in terms of their increased responses to external auditory stimuli.

Intrastratial photostimulation of corticostriatal, thalamostriatal, and nigrostriatal projections induces wakefulness

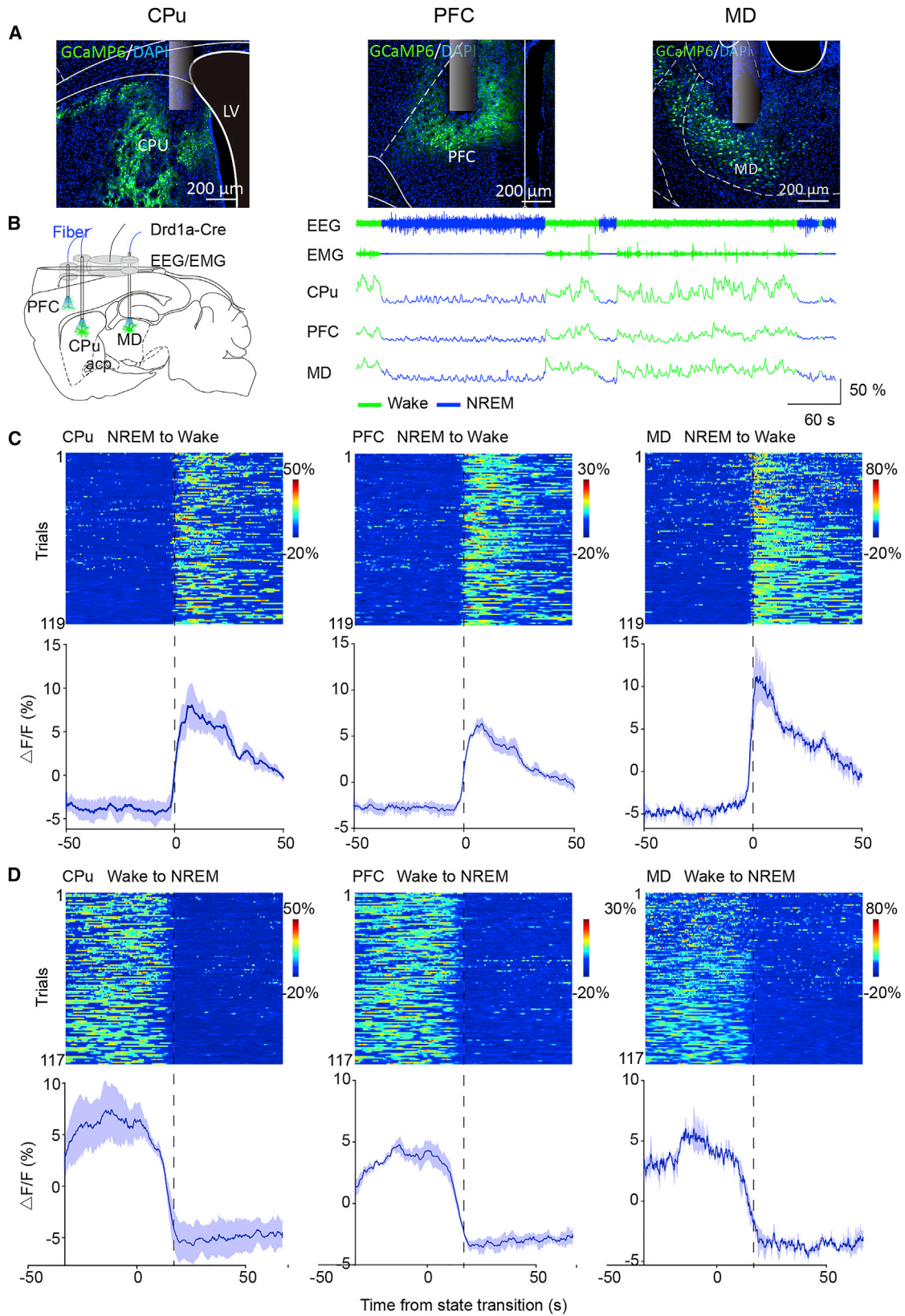
To investigate the individual contributions of PFC, MD, and SNc inputs to the dorsal striatum in inducing wakefulness, we injected an AAV expressing ChR2-mCherry under the control of the CaMKII promoter into the PFC or MD to target corticostriatal or thalamostriatal projections, respectively, in wild-type mice (Figures 5A and 5D). To target nigrostriatal projections, we injected an AAV virus expressing ChR2 in a Cre-dependent manner into the SNc of TH-Cre mice (Figure 5G). For photostimulation of the axonal terminals in the dorsal striatum from the PFC, MD, and SNc, each mouse was chronically implanted with a fiber optic probe into the dorsal striatum. Intrastratial photostimulation (470 nm, at 1–30 Hz for 10 s) of corticostriatal, thalamostriatal, and nigrostriatal projections decreased the EEG delta power and increased both EMG tone and the probability of wakefulness

Figure 3. Population activities of corticostriatal and thalamostriatal neurons, afferents of the dorsal striatum, across sleep states and in response to salient stimuli

(A and C) Viral-based retrograde-labeling approach to record the activities of corticostriatal and thalamostriatal neurons. Left: labeling of corticostriatal (A) or thalamostriatal (C) neurons via dorsal-striatal injections of AAV2-retro-hSyn-tdTomato-P2A-Cre and PFC (A) or MD (C) injections of AAV9-hSyn-DIO-GCaMP6f. Right: GCaMP6f expression in the PFC (A) or MD (C).

(B and D) Population activities of corticostriatal (B) or thalamostriatal (D) neurons across state transitions. Top: individual state transitions with color-coded fluorescent intensities. Bottom: average responses of all the state transitions expressed as the mean (blue) \pm SEM (shaded).

(E–P) Population activity of corticostriatal or thalamostriatal neurons in response to acute auditory tones during sleep (E–G) or wakefulness (H and I), as well as during foot shocks (K–M) and air puffs (N–P). (E, H, K, and N) Schematic showing application of acute auditory tones, foot shocks, and air puffs. (F, G, I, J, L, M, O, and P) Left: the time course of the calcium signals of corticostriatal or thalamostriatal neurons in response to stimuli. Right: average fluorescence before and after onset of the auditory tone when mice were asleep (F, $t_5 = 5.589$, $p = 0.00253$, G, $t_4 = 2.975$, $p = 0.0409$), or awake (I, $t_5 = 3.392$, $p = 0.0194$, J, $t_4 = 4.292$, $p = 0.0127$), as well as during foot shocks (L, $t_5 = 2.949$, $p = 0.0319$, M, $t_4 = 2.802$, $p = 0.0487$), or air puffs (O, $t_5 = 2.746$, $p = 0.0405$, P, $t_4 = 2.849$, $p = 0.0464$). See also Figures S1 and S2.



(legend on next page)

(Figures 5B, 5E, and 5H). The latency of the transition from NREM sleep to wakefulness was shortened in PFC-ChR2 (Figure 5C; $F_{1,9} = 395.27$, $p = 9.568 \times 10^{-9}$) or MD-ChR2 (Figure 5F; $F_{1,11} = 70.49$, $p = 4.115 \times 10^{-6}$) mice, compared with that of mCherry controls, in a stimulation-frequency-dependent manner. Photostimulation of corticostriatal projections at 1, 5, 10, 20, and 30 Hz in PFC-ChR2 mice shortened the latencies from NREM sleep to wakefulness—compared with those in PFC-mCherry mice—by 32%, 55%, 88%, 90%, and 98%, respectively. Photostimulation of thalamostriatal projections at 1, 5, 10, 20, and 30 Hz in MD-ChR2 mice shortened the latencies from NREM sleep to wakefulness—compared with those in MD-mCherry mice—by 16.8%, 33.3%, 78.7%, 80.4%, and 66.7%, respectively. The latencies from NREM-to-wake transitions were reduced in TH-ChR2 mice but not in TH-mCherry mice (Figure 5I; $F_{1,16} = 21.69$, $p = 0.0003$). However, this facilitation in NREM-to-wake transitions did not occur in a frequency-dependent manner ($F_{4,64} = 0.539$, $p = 0.707$). Next, we analyzed the arousal-promoting efficacy of each projection. The arousal-promoting efficacy of the corticostriatal projection was the strongest, whereas that of the nigrostriatal projection was the weakest ($F_{2,22} = 16.231$, $p = 4.673 \times 10^{-5}$). Taken together, intrastriatal photostimulation of corticostriatal, thalamostriatal, or nigrostriatal projections was sufficient to induce wakefulness.

Striatal D₁R neurons control wakefulness via the EP and SNr

To elucidate the downstream targets of striatal D₁R neurons in the modulation of wakefulness, we injected a Cre-dependent ChR2 virus into the dorsal striatum of *Drd1a*-Cre mice and bilaterally implanted fiber optic cannulae to target either the entopeduncular nucleus (EP, also called internal segment of the globus pallidus, GPi) or substantia nigra pars reticulata (SNr) (Figures 6A and 6D), both of which are efferent targets of striatal D₁R neurons. During NREM sleep, photostimulation (470-nm blue laser at 20 Hz) of striato-entopeduncular or striatonigral projections in ChR2 mice decreased EEG delta power and increased EMG tone (Figure 6B). Optogenetic activation of striato-entopeduncular projections increased the probability of wakefulness at the expense of NREM sleep (Figure 6B), as well as reduced the latency from NREM sleep to wakefulness, in D1-ChR2 mice compared with these parameters in mCherry control mice (Figure 6C; $t_9 = 19.01$, $p = 1.420 \times 10^{-8}$). Photostimulation (20 Hz) of striato-entopeduncular projections shortened the latency from NREM sleep to wakefulness by 87% in D1-ChR2 mice (7.3 ± 1.8 s) compared with that in D1-mCherry mice (57.7 ± 1.9 s). Optogenetic activation of striatonigral projections increased the probability of wakefulness at the expense of NREM sleep (Figure 6E) and also reduced the latency from

NREM sleep to wakefulness in D1-ChR2 mice compared with these parameters in mCherry control mice (Figure 6F; $t_{10} = 7.99$, $p = 1.192 \times 10^{-5}$). Photostimulation (20 Hz) of striatonigral projections shortened the latency from NREM sleep to wakefulness by 73% in D1-ChR2 mice (13.6 ± 3.7 s) compared with that in D1-mCherry mice (50.9 ± 1.9 s). Our findings indicated that optogenetic activation of either striato-entopeduncular or striatonigral projections from striatal D₁R neurons was sufficient to induce wakefulness.

Inhibition of striatal D₁R neurons attenuates wakefulness

Finally, to test the effects of striatal D₁R neurons in control of sleep-wake states by inhibition of these neurons, we employed an inhibitory chemogenetic element hM4Di. An AAV encoding modified inhibitory muscarinic M4 receptors by a Cre-dependent manner was injected into the dorsal striatum of *Drd1a*-Cre mice (Figure 7A). Robust expression of hM4Di receptors was observed in the dorsal striatum (Figure 7B). Following injections of CNO at 19:00 (mouse active period), NREM sleep was significantly increased over the 3-h post-injection period as compared with saline ($F_{1,7} = 15.946$, $p = 0.005$), and wakefulness was significantly attenuated ($F_{1,7} = 15.477$, $p = 0.006$; Figures 7C and 7D). Injections of CNO increased the amount of NREM sleep by 66.1% as compared with saline over the 3-h post-injection period (19:00–22:00) and reduced the amount of wakefulness by 28.9% over the 3-h post-injection period (Figure 7D). These findings demonstrate that inhibition of striatal D₁R neurons increases NREM sleep and attenuates wakefulness.

DISCUSSION

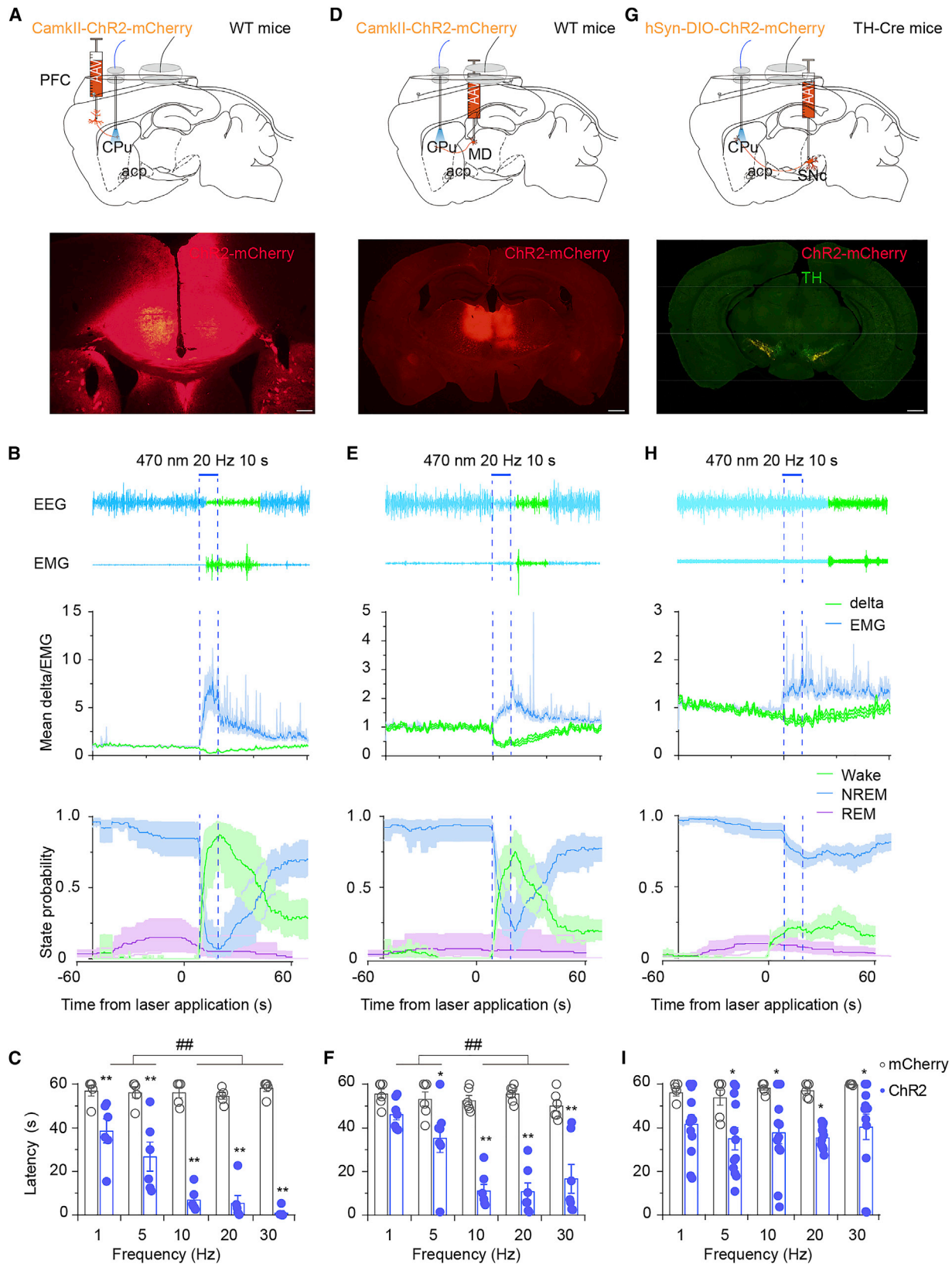
In this study, we found that activation of striatal D₁R neurons induced an immediate switch from NREM sleep to wakefulness and that striatal D₁R neurons were more active during wakefulness. Furthermore, the activities of striatal D₁R neurons were synchronized with those of corticostriatal neurons and thalamostriatal neurons. Intrastriatal optogenetic activation of corticostriatal, thalamostriatal, or nigrostriatal projections or stimulation of either striato-entopeduncular or striatonigral projections during NREM sleep produced an immediate NREM sleep-wakefulness transition. The upstreams and downstreams of striatal D₁R neurons constituted an up-down circuit for controlling wakefulness. Our findings revealed a circuit regulating wakefulness through striatal D₁R neurons.

Top-down pathway in control of wakefulness

Top-down signals from prefrontal cortex are implicated in numerous neurobiological processes—including attention,

Figure 4. Simultaneous neural population activities of striatal D₁R neurons and neurons in the prefrontal cortex and medial dorsal nucleus measured by multichannel fiber photometry across brain states

- (A) Expression of GCaMP6f in the dorsal striatum, PFC, and MD of a *Drd1a*-Cre mouse (scale bar, 200 μ m).
(B) Schematic showing fiber implantations in the dorsal striatum, PFC, and MD with simultaneous polysomnographic recordings in *Drd1a*-Cre mice (left). Right: example traces of EEG, EMG, and fluorescent signals across spontaneous sleep-wake states.
(C) Individual transitions from NREM sleep to wakefulness with color-coded fluorescent intensities (top). Average responses from all the state transitions (bottom) expressed as the mean (blue) \pm SEM (shaded).
(D) Individual transitions from wakefulness to NREM sleep with color-coded fluorescent intensities (top). Average responses from all the state transitions (bottom) expressed as the mean (blue) \pm SEM (shaded). See also Figures S3–S5.



(legend on next page)

memory, and consciousness—that are based upon heightened states of wakefulness. However, such top-down circuits have rarely been investigated in the context of sleep-wake regulation.²² Classical arousal circuitry is composed of ascending systems arising from bottom-up signals from the pons to the cortex, which synapse and signal in the midbrain and diencephalon en route to the cortex.²³ The dorsal striatum receives excitatory input from almost all regions of the cerebral cortex,²⁴ as well as from many thalamic nuclei.²⁵ In contrast, long-distance inhibitory inputs to the dorsal striatum have rarely been reported. Moreover, MSNs are characterized by their negative resting membrane potentials and low firing rates.¹⁷ Based on these findings, it is likely that the activities of striatal MSNs are primarily controlled by excitatory inputs from the cerebral cortex, thalamus, or dopaminergic inputs from the SNc. Cortical neuronal activity is necessary for dorsal-striatal neuronal activity (c-fos level), and the cortex shapes dorsal-striatal activity via signaling from NMDA receptors.²⁶ In the present study, we applied cell-type-specific fiber photometry to simultaneously monitor the population activities of corticostriatal neurons, thalamostriatal neurons, and striatal D₁R neurons and found that the activities of striatal D₁R neurons were synchronized with their afferent populations during spontaneous sleep-wake states and in response to external salient events. Moreover, optogenetic stimulation of corticostriatal projections induced a rapid switch from NREM sleep to wakefulness. Therefore, we confirmed that corticostriatal projections predominated the activities of striatal D₁R neurons. Photostimulation of either striatal D₁R neurons or corticostriatal, striato-entopeduncular, or striatonigral projections induced rapid NREM-to-wake transitions. Hence, we conclude that the top-down arousal signal from prefrontal cortex to subcortex via the dorsal striatum is crucial for wakefulness.

Functional dichotomy of the dorsal striatum in sleep-wake regulation

Clinical features have associated the dorsal striatum with sleep disturbances in PD.¹ Pharmacological agents that systemically target dopamine or adenosine receptors, which are densely expressed in the striatum, potentially alter sleep-wake cycles.^{27,28} Additionally, striatal lesions disrupt sleep.^{29,30} Genetically modified animal models and functional neuroimaging of normal human sleep via PET^{3–5} strongly implicate the dorsal striatum in sleep-wake regulation. However, the roles of the dorsal striatum in sleep regulation have not been fully elucidated, as previous studies have been unable to specifically target the two morphologically indistinguishable and mosaically distributed MSN subtypes. Compared with traditional methods that lack cellular specificity, recently developed optogenetic and chemogenetic technologies combined with cell-type-specific

transgenic animal lines have enabled precise manipulations of the activities of specific neurons with high spatiotemporal resolution to dissect striatal subpopulations underlying sleep-wake regulation.³¹ Our previous study showed that chemogenetic activation of striatal D₂R/A_{2A}R neurons induced a remarkable increase in NREM sleep via the external globus pallidus.³² In this study, optogenetic activation of striatal D₁R neurons promoted wakefulness. Consistent with functional neuroimaging of normal human sleep and c-fos expression in animals,^{3–6,26,33} our photometry data in this study demonstrated that striatal D₁R neurons were more active during wakefulness than during sleep. Our previous and present findings demonstrate opposing contributions of striatal D₁R neurons and D₂R neurons to sleep-wake regulation, highlighting a functional dichotomy between these two distinct subpopulations of MSNs in the dorsal striatum. Striatal D₁R neurons directly project to the output nuclei of the basal ganglia (BG) (the EP and SNr); in contrast, striatal D₂R/A_{2A}R neurons indirectly influence SNr and EP activities via the external globus pallidus.^{34,35} The output nuclei of the BG send their inhibitory projections to the pedunculo-pontine tegmental nucleus (PPTg), which is the principal component of the ascending arousal system.^{36,37} In the present study, photostimulation of striatal D₁R soma or their axonal terminals in the EP or SNr induced wakefulness. Taken together, we conclude that wakefulness is driven by the activation of GABAergic striatal D₁R neurons inhibiting the EP and SNr, which may lead to disinhibition of PPTg neurons.

Comparison of D₁R neurons in the nucleus accumbens (NAc) and dorsal striatum

The NAc is the major component of the ventral striatum and has been implicated in mediating motivation, reward, and feeding.³⁸ Lesions of the NAc result in increases in wakefulness, whereas striatal lesions decrease and destabilize wakefulness in rats,^{30,39} suggesting that the NAc predominates sleep, whereas the dorsal striatum predominates wakefulness. In the present study, we found that striatal D₁R neurons were most active during wakefulness, and activation of striatal D₁R neurons produced immediate NREM-to-wake transitions. In contrast, our previous study showed that the activity of NAc D₁R neurons is the highest during REM sleep.¹⁶ Moreover, NAc and striatal D₁R neurons have distinct afferents and efferents from one another. The NAc receives robust dopaminergic inputs from the VTA, whereas the dorsal striatum receives dopaminergic inputs primarily from the SNc.⁴⁰ In the present study, photostimulation of dopaminergic terminals in the dorsal striatum mildly reduced the latency to awake from NREM sleep via outputs to the EP and SNr. Taken together, although both NAc and striatal D₁R neurons promote wakefulness, their contributions are mediated via distinct afferent and efferent pathways.

Figure 5. Photostimulation of corticostriatal, thalamostriatal, or nigrostriatal projections promotes wakefulness

(A, D, and G) Schematic showing injection of Cre-independent AAVs expressing ChR2-mCherry under the CaMKII promoter in the PFC (A) or MD (D), or Cre-inducible AAVs expressing ChR2-mCherry under the hSyn promoter into the SNc (G), as well as laser application with simultaneous polysomnographic recordings and ChR2 expression at injection sites. Scale bars, 200 μ m (A) and 600 μ m (D and G).

(B, E, and H) Typical trials of optogenetic stimulation (20 Hz, 5-ms pulse duration, total 10 s) of the PFC (B), MD (E), or SNc (H), and the mean delta power of EEGs (green line), integral of EMGs (blue line), or state probabilities before, during, and after laser stimulation.

(C, F, and I) The latency of transitions from NREM sleep to wakefulness induced by blue-light photostimulation of the PFC (C, $F_{1,9} = 395.27$, $p = 9.568 \times 10^{-9}$), MD (F, $F_{1,11} = 70.49$, $p = 4.115 \times 10^{-6}$) or SNc (I, $F_{1,16} = 21.69$, $p = 0.0003$) with different frequencies (1–30 Hz).

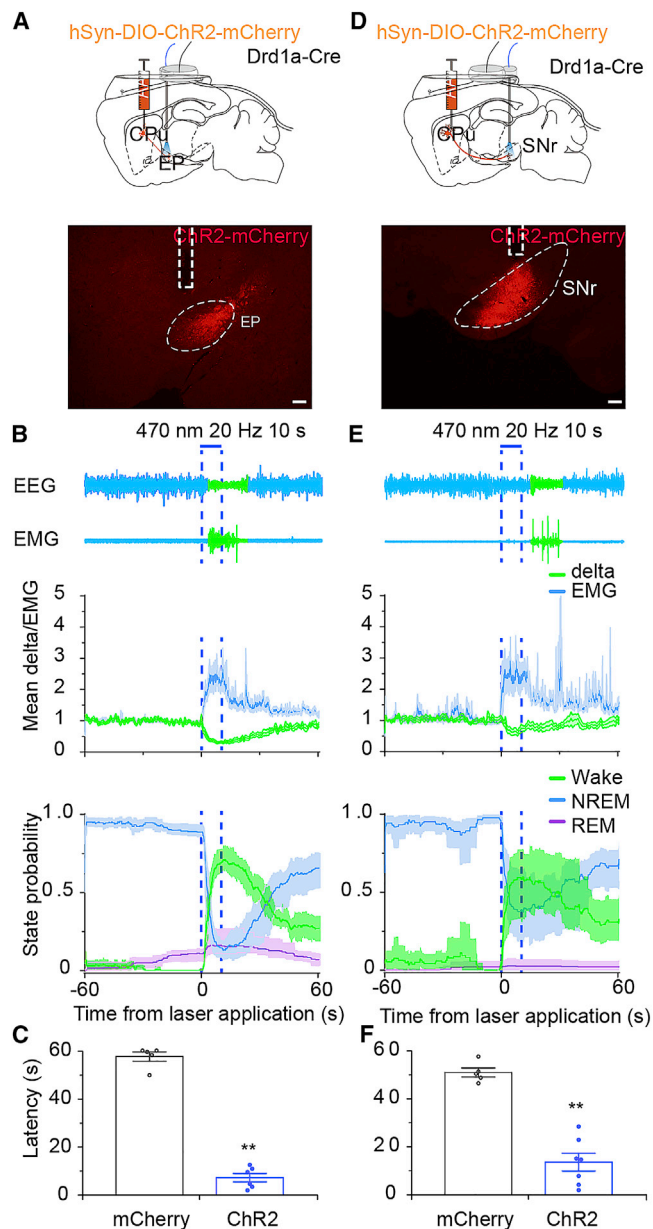


Figure 6. Photostimulation of striato-entopeduncular or striatonigral projections promotes wakefulness

(A and D) Schematic showing injection of Cre-inducible AAVs expressing ChR2-mCherry into the dorsal striatum and implantation of optical fibers into the EP (A) or SNr (D), as well as simultaneous polysomnographic recordings. Representative images of striato-entopeduncular (A) or striatonigral (D) fibers expressing ChR2-mCherry at the EP (A) or SNr (D) (scale bar, 200 μ m). (B and E) Typical EEG and EMG traces during optogenetic stimulation (20 Hz, 5-ms pulse duration, total 10 s) of striato-entopeduncular (B) or striatonigral (E) axonal terminals. Mean delta power of EEGs (green line) or EMG integrals (blue line), as well as state probabilities before, during, and after laser stimulation of striato-entopeduncular (B) or striatonigral (E) axonal terminals are shown. (C and F) Latencies of transitions from NREM sleep to wakefulness induced by blue-light photostimulation of striato-entopeduncular (C, $t_9 = 19.01$, $p = 1.420 \times 10^{-8}$) or striatonigral (F, $t_{10} = 7.99$, $p = 1.192 \times 10^{-5}$) axonal terminals.

Implications of the dorsal striatum as a target for treatment of excessive daytime sleepiness

EDS is a common complaint among PD patients.¹ The prevailing model of PD asserts that loss of dopamine elevates the efficacy of striatopallidal neurons and/or decreases the efficacy of the striatonigral neurons, which results in an imbalance in the contributions of these neurons in the control of BG output.⁴¹ In hemi-parkinsonian rats, striatonigral neurons have been shown to be inhibited, whereas striatopallidal neurons have been found to be activated.⁴² Parker and colleagues found that dopaminergic deletion selectively decreased the synaptic strengths of thalamic excitatory inputs to D₁R neurons but not D₂R/A_{2A}R neurons, while modulation of thalamostriatal synapses rescued PD motor deficits.⁴³ The selective D₁R agonist, SKF38393, efficiently alleviated EDS and restored daytime napping to baseline physiologic levels in Parkinsonian macaque monkeys.⁸ Combined with our present results about D₁R neurons promoting wakefulness, we conclude that elevating the activities of striatopallidal neurons increases sleep-promoting efficacies, whereas lowering the activities of striatonigral neurons decreases wake-promoting efficacies, which may underlie EDS in PD patients. Thus, restoring the balance of contributions from striatonigral and striatopallidal neurons may represent a novel treatment strategy for EDS in PD patients.

In summary, our findings demonstrate the importance of striatal D₁R neurons in the control of wakefulness and reveal a top-down pathway from cortex to subcortex. The roles of striatal D₁R neurons in sleep-wake regulation may greatly facilitate the development of treatments for sleep disorders in PD patients.

STAR★METHODS

Detailed methods are provided in the online version of this paper and include the following:

- KEY RESOURCES TABLE
- RESOURCE AVAILABILITY
 - Lead contact
 - Materials availability
 - Data and code availability
- EXPERIMENTAL MODEL AND SUBJECT DETAILS
 - Mice
- METHOD DETAILS
 - Surgery
 - Preparation of AAVs
 - Electrode implantations for electroencephalography/electromyography (EEG/EMG)
 - Polysomnographic recordings and analysis
 - Photostimulation
 - Fiber photometry
 - Chemicals and drug administrations
 - Auditory tone test
 - Electric footshocks
 - Air puffs
 - Histology
- QUANTIFICATION AND STATISTICAL ANALYSIS

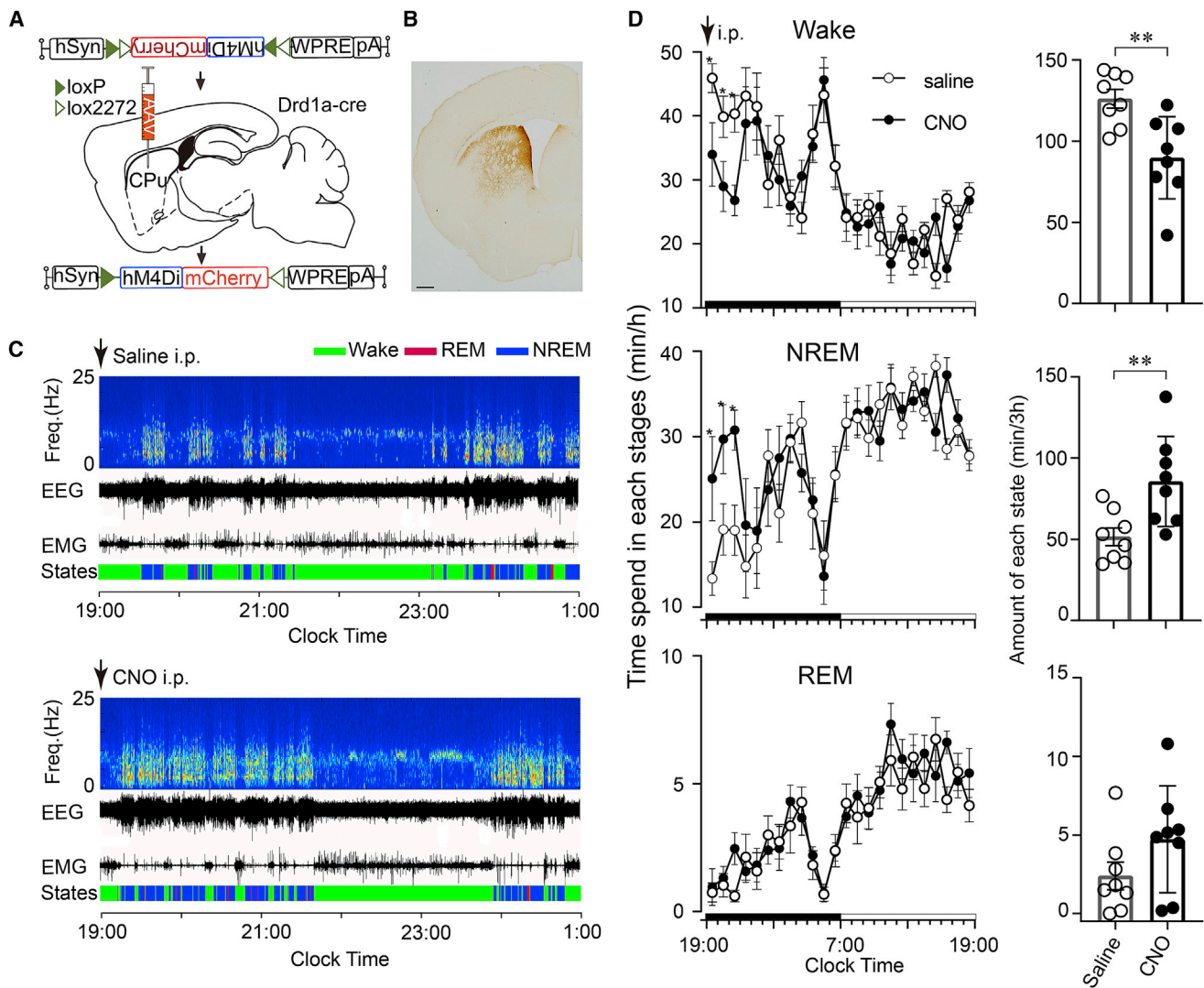


Figure 7. Chemogenetic inhibition of striatal D₁R neurons attenuates wakefulness

(A) Schematic of Cre-inducible adeno-associated viruses expressing hM4Di-mCherry targeting to the dorsal striatum of *Drd1a*-Cre mice.

(B) The expression of hM4Di in the dorsal striatum. Scale bar, 500 μ m.

(C) Typical examples of EEG power spectrogram, EEG, EMG and hypnograms over 6 h following saline (up) or CNO (1 mg \cdot kg⁻¹, i.p., down) administration in a *Drd1a*-Cre mouse with bilateral hM4Di expression in the dorsal striatum.

(D) Left: the time course changes of wakefulness, NREM and REM sleep profiles after injection of CNO or saline. Open and shaded cycles show the saline-group and CNO-group profiles, respectively. Values are means \pm SEM (n = 8). *p < 0.05, **p < 0.01, significantly different from the corresponding saline. Right: total time spent in each state over the first 3 h (19:00–22:00).

SUPPLEMENTAL INFORMATION

Supplemental information can be found online at <https://doi.org/10.1016/j.cub.2021.12.026>.

ACKNOWLEDGMENTS

This study was supported by the National Major Project of China Science and Technology Innovation 2030 for Brain Science and Brain-Inspired Technology (2021ZD0203400 to Z.-L.H.), National Key Research and Development Program of China (2020YFC2005300 to W.-M.Q.), the National Natural Science Foundation of China (82020108014 and 32070984 to Z.-L.H.; 82071491 and 31871072 to W.-M.Q.; 31971110 and 32171142 to X.-S.Y.), the Shanghai Science and Technology Innovation Action Plan Laboratory Animal Research

Project (201409001800 to Z.-L.H.), Program for Shanghai Outstanding Academic Leaders (to Z.-L.H.), the Shanghai Municipal Science and Technology Major Project, and ZJLab (2018SHZDZX01 to Z.-L.H.).

AUTHOR CONTRIBUTIONS

H.D., W.-M.Q., and Z.-L.H. designed the experiments. H.D., Z.-K.C., H.G., and X.-S.Y. performed the optogenetic and chemogenetic manipulation experiments. H.D., H.G., Z.-K.C., and C.-W.L. performed the fiber photometry recording and behavioral experiments. H.D., Z.-K.C., and H.G. performed and analyzed immunohistochemistry. H.D., Z.-K.C., H.G., and X.-S.Y. analyzed and interpreted the data. H.D., Z.-K.C., and Z.-L.H. wrote and revised the manuscript. W.-M.Q. and Z.-L.H. supervised the study and acquired funding.

DECLARATION OF INTERESTS

The authors declare no competing interests.

Received: June 30, 2021

Revised: October 17, 2021

Accepted: December 9, 2021

Published: January 11, 2022

REFERENCES

- Adler, C.H., and Thorpy, M.J. (2005). Sleep issues in Parkinson's disease. *Neurology* 64, S12–S20.
- Knie, B., Mitra, M.T., Logishetty, K., and Chaudhuri, K.R. (2011). Excessive daytime sleepiness in patients with Parkinson's disease. *CNS Drugs* 25, 203–212.
- Braun, A.R., Balkin, T.J., Wesenten, N.J., Carson, R.E., Varga, M., Baldwin, P., Selbie, S., Belenky, G., and Herscovitch, P. (1997). Regional cerebral blood flow throughout the sleep-wake cycle. An H₂(15)O PET study. *Brain* 120, 1173–1197.
- Maquet, P., Degueldre, C., Delfiore, G., Aerts, J., Péters, J.M., Luxen, A., and Franck, G. (1997). Functional neuroanatomy of human slow wave sleep. *J. Neurosci.* 17, 2807–2812.
- Kajimura, N., Uchiyama, M., Takayama, Y., Uchida, S., Uema, T., Kato, M., Sekimoto, M., Watanabe, T., Nakajima, T., Horikoshi, S., et al. (1999). Activity of midbrain reticular formation and neocortex during the progression of human non-rapid eye movement sleep. *J. Neurosci.* 19, 10065–10073.
- Dang-Vu, T.T., Desseilles, M., Laureys, S., Degueldre, C., Perrin, F., Phillips, C., Maquet, P., and Peigneux, P. (2005). Cerebral correlates of delta waves during non-REM sleep revisited. *Neuroimage* 28, 14–21.
- Hurley, M.J., Mash, D.C., and Jenner, P. (2001). Dopamine D1 receptor expression in human basal ganglia and changes in Parkinson's disease. *Mol. Brain Res.* 87, 271–279.
- Hyacinthe, C., Barraud, Q., Tison, F., Bezard, E., and Ghorayeb, I. (2014). D1 receptor agonist improves sleep-wake parameters in experimental parkinsonism. *Neurobiol. Dis.* 63, 20–24.
- Ongini, E., Caporali, M.G., and Massotti, M. (1985). Stimulation of dopamine D-1 receptors by SKF 38393 induces EEG desynchronization and behavioral arousal. *Life Sci* 37, 2327–2333.
- Ongini, E., and Caporali, M.G. (1987). Differential effects of dopamine D-1 and D-2 receptor agonists on EEG activity and behaviour in the rabbit. *Neuropharmacology* 26, 355–360.
- Kropf, W., and Kuschinsky, K. (1993). Effects of stimulation of dopamine D1 receptors on the cortical EEG in rats: different influences by a blockade of D2 receptors and by an activation of putative dopamine autoreceptors. *Neuropharmacology* 32, 493–500.
- Monti, J.M., Fernández, M., and Jantos, H. (1990). Sleep during acute dopamine D1 agonist SKF 38393 or D1 antagonist SCH 23390 administration in rats. *Neuropsychopharmacology* 3, 153–162.
- Madisen, L., Mao, T., Koch, H., Zhuo, J.M., Berenyi, A., Fujisawa, S., Hsu, Y.W., Garcia, A.J., 3rd, Gu, X., Zanella, S., et al. (2012). A toolbox of Cre-dependent optogenetic transgenic mice for light-induced activation and silencing. *Nat. Neurosci.* 15, 793–802.
- Gong, S., Zheng, C., Doughty, M.L., Losos, K., Didkovsky, N., Schambra, U.B., Nowak, N.J., Joyner, A., Leblanc, G., Hatten, M.E., and Heintz, N. (2003). A gene expression atlas of the central nervous system based on bacterial artificial chromosomes. *Nature* 425, 917–925.
- Li, Y., Zhong, W., Wang, D., Feng, Q., Liu, Z., Zhou, J., Jia, C., Hu, F., Zeng, J., Guo, Q., et al. (2016). Serotonin neurons in the dorsal raphe nucleus encode reward signals. *Nat. Commun.* 7, 10503.
- Luo, Y.J., Li, Y.D., Wang, L., Yang, S.R., Yuan, X.S., Wang, J., Cherasse, Y., Lazarus, M., Chen, J.F., Qu, W.M., and Huang, Z.-L. (2018). Nucleus accumbens controls wakefulness by a subpopulation of neurons expressing dopamine D1 receptors. *Nat. Commun.* 9, 1576.
- Kreitzer, A.C., and Malenka, R.C. (2008). Striatal plasticity and basal ganglia circuit function. *Neuron* 60, 543–554.
- Liu, X.B., and Murray, K.D. (2012). Neuronal excitability and calcium/calmodulin-dependent protein kinase type II: location, location, location. *Epilepsia* 53, 45–52.
- Hunnicutt, B.J., Long, B.R., Kusefoglu, D., Gertz, K.J., Zhong, H., and Mao, T. (2014). A comprehensive thalamocortical projection map at the mesoscopic level. *Nat. Neurosci.* 17, 1276–1285.
- Yao, Z., van Velthoven, C.T.J., Nguyen, T.N., Goldy, J., Sedeno-Cortes, A.E., Baftizadeh, F., Bertagnoli, D., Casper, T., Chiang, M., Crichton, K., et al. (2021). A taxonomy of transcriptomic cell types across the isocortex and hippocampal formation. *Cell* 184, 3222–3241, e3226.
- Lui, J.H., Nguyen, N.D., Grutzner, S.M., Darmanis, S., Peixoto, D., Wagner, M.J., Allen, W.E., Kebschull, J.M., Richman, E.B., Ren, J., et al. (2021). Differential encoding in prefrontal cortex projection neuron classes across cognitive tasks. *Cell* 184, 489–506, e26.
- Uygun, D.S., Ye, Z., Zecharia, A.Y., Harding, E.C., Yu, X., Yustos, R., Vyssotski, A.L., Brickley, S.G., Franks, N.P., and Wisden, W. (2016). Bottom-up versus top-down induction of sleep by zolpidem acting on histaminergic and neocortex neurons. *J. Neurosci.* 36, 11171–11184.
- Saper, C.B., Scammell, T.E., and Lu, J. (2005). Hypothalamic regulation of sleep and circadian rhythms. *Nature* 437, 1257–1263.
- Mink, J.W. (1996). The basal ganglia: focused selection and inhibition of competing motor programs. *Prog. Neurobiol.* 50, 381–425.
- Wall, N.R., De La Parra, M., Callaway, E.M., and Kreitzer, A.C. (2013). Differential innervation of direct- and indirect-pathway striatal projection neurons. *Neuron* 79, 347–360.
- Qiu, M.H., Chen, M.C., Huang, Z.L., and Lu, J. (2014). Neuronal activity (c-Fos) delineating interactions of the cerebral cortex and basal ganglia. *Front. Neuroanat.* 8, 13.
- Huang, Z.L., Qu, W.M., Eguchi, N., Chen, J.F., Schwarzschild, M.A., Fredholm, B.B., Urade, Y., and Hayaishi, O. (2005). Adenosine A2A, but not A1, receptors mediate the arousal effect of caffeine. *Nat. Neurosci.* 8, 858–859.
- Qu, W.M., Huang, Z.L., Xu, X.H., Matsumoto, N., and Urade, Y. (2008). Dopaminergic D1 and D2 receptors are essential for the arousal effect of modafinil. *J. Neurosci.* 28, 8462–8469.
- Mena-Segovia, J., Cintra, L., Prospéro-García, O., and Giordano, M. (2002). Changes in sleep-waking cycle after striatal excitotoxic lesions. *Behav. Brain Res.* 136, 475–481.
- Qiu, M.H., Vetrivelan, R., Fuller, P.M., and Lu, J. (2010). Basal ganglia control of sleep-wake behavior and cortical activation. *Eur. J. Neurosci.* 31, 499–507.
- Deisseroth, K. (2015). Optogenetics: 10 years of microbial opsins in neuroscience. *Nat. Neurosci.* 18, 1213–1225.
- Yuan, X.S., Wang, L., Dong, H., Qu, W.M., Yang, S.R., Cherasse, Y., Lazarus, M., Schiffmann, S.N., d'Exaerde, A.K., Li, R.X., and Huang, Z.-L. (2017). Striatal adenosine A2a receptor neurons control active-period sleep via parvalbumin neurons in external globus pallidus. *eLife* 6.
- Sastre, J.P., Buda, C., Lin, J.S., and Jouvet, M. (2000). Differential c-fos expression in the rhinencephalon and striatum after enhanced sleep-wake states in the cat. *Eur. J. Neurosci.* 12, 1397–1410.
- Lukhanina, E.P., Kolomiets, B.P., and Pil'kevich, N.A. (2001). Role of neostriatal dopamine D1 and D2 receptors in the organization of neuronal activity in the entopeduncular nucleus. *Neurophysiology* 33, 249–257.
- Freeze, B.S., Kravitz, A.V., Hammack, N., Berke, J.D., and Kreitzer, A.C. (2013). Control of basal ganglia output by direct and indirect pathway projection neurons. *J. Neurosci.* 33, 18531–18539.
- Roseberry, T.K., Lee, A.M., Lalive, A.L., Wilbrecht, L., Bonci, A., and Kreitzer, A.C. (2016). Cell-type-specific control of brainstem locomotor circuits by basal ganglia. *Cell* 164, 526–537.
- Kroeger, D., Ferrari, L.L., Petit, G., Mahoney, C.E., Fuller, P.M., Arrigoni, E., and Scammell, T.E. (2017). Cholinergic, glutamatergic, and GABAergic

- neurons of the pedunculopontine tegmental nucleus have distinct effects on sleep/wake behavior in mice. *J. Neurosci.* **37**, 1352–1366.
38. Salgado, S., and Kapliitt, M.G. (2015). The nucleus accumbens: a comprehensive review. *Stereotact. Funct. Neurosurg.* **93**, 75–93.
 39. Qiu, M.H., Liu, W., Qu, W.M., Urade, Y., Lu, J., and Huang, Z.L. (2012). The role of nucleus accumbens core/shell in sleep-wake regulation and their involvement in modafinil-induced arousal. *PLoS One* **7**, e45471.
 40. Poulin, J.F., Caronia, G., Hofer, C., Cui, Q., Helm, B., Ramakrishnan, C., Chan, C.S., Dombeck, D.A., Deisseroth, K., and Awatramani, R. (2018). Mapping projections of molecularly defined dopamine neuron subtypes using intersectional genetic approaches. *Nat. Neurosci.* **21**, 1260–1271.
 41. Albin, R.L., Young, A.B., and Penney, J.B. (1989). The functional anatomy of basal ganglia disorders. *Trends Neurosci* **12**, 366–375.
 42. Mallet, N., Ballion, B., Le Moine, C., and Gonon, F. (2006). Cortical inputs and GABA interneurons imbalance projection neurons in the striatum of parkinsonian rats. *J. Neurosci.* **26**, 3875–3884.
 43. Parker, P.R., Lalive, A.L., and Kreitzer, A.C. (2016). Pathway-specific remodeling of thalamostriatal synapses in parkinsonian mice. *Neuron* **89**, 734–740.
 44. Yang, S.R., Hu, Z.Z., Luo, Y.J., Zhao, Y.N., Sun, H.X., Yin, D., et al. (2018). The rostromedial tegmental nucleus is essential for non-rapid eye movement sleep. *PLoS Biol.* **16**, e2002909.
 45. Zhang, Z., Wang, H.J., Wang, D.R., Qu, W.M., and Huang, Z.L. (2017). Red light at intensities above 10 lx alters sleep-wake behavior in mice. *Light Sci. Appl.* **6**, e16231.
 46. Dong, H., Wang, J., Yang, Y.F., Shen, Y., Qu, W.M., and Huang, Z.L. (2019). Dorsal striatum dopamine levels fluctuate across the sleep-wake cycle and respond to salient stimuli in mice. *Front. Neurosci.* **13**, 242.
 47. Guo, Q., Zhou, J., Feng, Q., Lin, R., Gong, H., Luo, Q., Zeng, S., Luo, M., and Fu, L. (2015). Multi-channel fiber photometry for population neuronal activity recording. *Biomed. Opt. Express* **6**, 3919–3931.
 48. Cho, J.R., Treweek, J.B., Robinson, J.E., Xiao, C., Bremner, L.R., Greenbaum, A., and Gradinaru, V. (2017). Dorsal raphe dopamine neurons modulate arousal and promote wakefulness by salient stimuli. *Neuron* **94**, 1205–1219, e8.
 49. Eban-Rothschild, A., Rothschild, G., Giardino, W.J., Jones, J.R., and de Lecea, L. (2016). VTA dopaminergic neurons regulate ethologically relevant sleep-wake behaviors. *Nat. Neurosci.* **19**, 1356–1366.
 50. Weber, F., Chung, S., Beier, K.T., Xu, M., Luo, L., and Dan, Y. (2015). Control of REM sleep by ventral medulla GABAergic neurons. *Nature* **526**, 435–438.

STAR★METHODS

KEY RESOURCES TABLE

| REAGENT or RESOURCE | SOURCE | IDENTIFIER |
|------------------------------------------------------|--------------------------------------------------|-----------------------------------------------------------------------------------------------------------------------|
| Antibodies | | |
| rabbit anti-tyrosine hydroxylase | Millipore | Cat#: AB152; RRID: AB_390204 |
| rabbit anti-mCherry | Clontech | Cat#: 632496; RRID: AB_10013483 |
| donkey anti-rabbit Alexa Fluor 488 | Jackson ImmunoResearch | Cat#: 711-545-152; RRID: AB_2313584 |
| Biotinylated Donkey anti-rabbit IgG | Jackson ImmunoResearch | Cat#: 711-065-152; RRID: AB_2340593 |
| Bacterial and virus strains | | |
| AAV2/9-CamkII-ChR2(H134R)-mCherry | Taitool Bioscience | Cat.S0166-9 |
| AAV2/9-hEF1a-DIO-hChR2(H134R)-mCherry-WPRE-pA | Taitool Bioscience | Cat.S0170-9 |
| AAV2/9-CamkII-mCherry | Taitool Bioscience | Cat. S0242-9 |
| AAV2/9-hSyn-DIO-mCherry | Taitool Bioscience | Cat. S0240-9 |
| AAV2/9-hSyn-FLEX-GCaMP6f-WPRE-pA | Taitool Bioscience | Cat.S0226-9 |
| AAV2/9-CamkII-GCaMP6f | Taitool Bioscience | Cat. S0228-9 |
| AAV2-retro-hSyn-tdTomato-P2A-iCre | Taitool Bioscience | Cat. S0509-2R |
| AAV2/9-CamkII-hM4Di-mCherry | Taitool Bioscience | Cat. S0141-9 |
| AAV2/9-hsyn-DIO-hM4Di-mCherry | Taitool Bioscience | Cat. S0193-9 |
| AAV-EF1a-DIO-NES-jRCaMP1a-WPRE-hGH polyA | BrainVTA | Cat. PT-1162 |
| Chemicals, peptides, and recombinant proteins | | |
| Clozapine N-oxide | LKT Laboratories | Cat NO: C4759 |
| Experimental models: Organisms/strains | | |
| Mouse: Drd1a-Cre | Mutant Mouse Resource & Research Centers (MMRRC) | RRID: MMRRC_034259-UCD |
| Mouse: Ai32 | Jackson laboratory | RRID: IMSR_JAX:012569 |
| Mouse: TH-Cre | Yuqiang Ding | ⁴⁴ |
| Mouse: C57BL/6J | Slac Laboratory Animal, Shanghai | N/A |
| Software and algorithms | | |
| GraphPad Prism 7.0 | GraphPad Software | https://www.graphpad.com/scientific-software/prism/ |
| Sleepsign | KISSEI COMTEC | http://www.sleepsign.com/ |
| MATLAB R2016a | Mathworks | https://ww2.mathworks.cn/products/matlab.html |
| Spike2 | Cambridge Electronic Design | http://ced.co.uk/ |
| Adobe Illustrator CC | Adobe | https://www.adobe.com/ |
| Adobe Photoshop CC | Adobe | https://www.adobe.com/ |

RESOURCE AVAILABILITY

Lead contact

Further information and requests for resources and reagents should be directed to and will be fulfilled by the Lead Contact, Zhi-Li Huang (huangzl@fudan.edu.cn)

Materials availability

This study did not generate new unique reagents.

Data and code availability

Data reported in this paper will be shared by the lead contact upon request.

This paper does not report original code.

Any additional information required to reanalyze the data reported in this paper is available from the lead contact upon request.

EXPERIMENTAL MODEL AND SUBJECT DETAILS

Mice

*Drd1a-Cre*¹⁴ (EY266 line, GENSAT project) mice were kindly provided by Jiang-Fan Chen and were crossed with the channelrhodopsin (ChR2)-YFP reporter mouse line (Ai32, the Jackson laboratory, Stock No: 012569) to induce ChR2 expression in striatal D₁R neurons. Mice were housed at an ambient temperature of 22 ± 1°C at a relative humidity level of 55 ± 5% under a 12/12-h light/dark cycle (lights on at 7 a.m., illumination intensity ≈ 100 lx).⁴⁵ Food and water were available *ad libitum*. All experiments were carried out in accordance with the Animal Experiment and Use Committee at the Shanghai Medical School of Fudan University.

METHOD DETAILS

Surgery

Adult mice were anesthetized with sodium pentobarbital (intraperitoneal, 80 mg kg⁻¹) and 1% lidocaine hydrochloride (subcutaneous, under the scalp), and were then placed on a stereotaxic frame (RWD Life Science, China). Small craniotomy holes were made for viral injections. AAVs were microinjected through a fine glass pipette. A total of 200 nL of virus was delivered into the dorsal striatum (anteroposterior = 0.80 mm, mediolateral = ±1.60 mm, dorsoventral = -2.7 mm), PFC (AP=1.0 mm, ML=±0.3 mm, DV=-1.2 mm), MD (AP=-1.5 mm, ML=±0.4 mm, DV=-3.0) or SNc (AP=-3.2 mm, ML=± 1.5 mm, DV= -4.0 mm) over a 5-min period per site via nitrogen gas pulsed at 20 psi using an air compression system (Picospritzer III, Parker Hannifin), as previously described.^{32,46} After infusion, the pipette was kept at the injection site for at least 5 min and was then withdrawn slowly. An AAV encoding GCaMP6f was infused unilaterally into the dorsal striatum, PFC, MD or SNc, and an AAV encoding ChR2 was injected bilaterally into dorsal striatum, PFC, MD, or SNc. After injections, mice were placed on a heating pad for recovery. To allow time for viral expression, mice were housed for at least two weeks following viral injections.

Mice used for *in vivo* optogenetic or fiber photometry experiments were implanted with optical fiber cannulae (Fiber core: 200 μm; numerical aperture (NA): 0.37; Newdoon, China) over the dorsal striatum, PFC, MD, EP or SNr. The fiber cannulae for fiber photometry were implanted 0.2 mm above the viral injection sites. The fiber cannulae for optogenetic manipulations were implanted into the dorsal striatum (AP=0.80 mm, ML=±1.60mmDV=2.3 mm), EP (AP=-1.3 mm, ML= ±1.7 mm, DV= -3.7 mm) or SNr (AP=-3.2 mm, ML=± 1.5 mm, DV= -4.0 mm).

Preparation of AAVs

Recombinant AAV vectors carrying optogenetic or chemogenetic elements and their corresponding controls (AAV-hsyn-DIO-ChR2(H134R)-mCherry, AAV-hsyn-DIO-mCherry, AAV-CamkII-ChR2(H134R)-mCherry, AAV-CamkII-mCherry), AAV-hsyn-DIO-hM4Di-mCherry, AAV2/9-hsyn-DIO-hM4Di-mCherry, AAV-EF1a-DIO-NES-jRCaMP1a-WPRE-hGH polyA, as well as AAVs carrying calcium indicators (AAV-hsyn-DIO-GCaMP6f, AAV-CamkII-GCaMP6f), were serotyped with AAV9 coat proteins, retrograde tracing AAV (AAV2-retro-hSyn-tdTomato-P2A-iCre) were serotyped with AAV2/retro coat proteins and packaged by Taitool Bioscience (Shanghai, China). The final viral concentration of the calcium indicator was 5 × 10¹² genome copies (gc) ml⁻¹. The final viral concentration for optogenetics and chemogenetic were 2 × 10¹² gc ml⁻¹. The final viral concentration of retrograde AAV was 1.5 × 10¹³ gc ml⁻¹. Aliquots of AAVs were stored at -80°C until their use during stereotaxic injections.

Electrode implantations for electroencephalography/electromyography (EEG/EMG)

As our previous study described,^{32,46} the employed electrodes consisted of two stainless steel screws with wire leads for EEG recordings and two Teflon-coated stainless-steel wires (Cooner Wire, USA) for EMG recordings. To implant the electrodes, two small craniotomy holes were made in frontal (AP= +1.5 mm, ML= -1.0 mm) and parietal (AP= -1.5 mm, ML= -1.0 mm) regions with a cranial drill. The EEG electrodes were screwed into the craniotomy holes and the EMG wires were bilaterally placed into trapezius muscles. All electrodes were attached to a microconnector and were fixed to the skull with dental cement. Scalp wounds were then sutured with needle and thread. After injections, mice were placed on a heating pad for recovery.

Polysomnographic recordings and analysis

After 2–4 weeks of recovery, each animal was connected to an EEG/EMG recording cable in a recording cage (transparent barrels) and was habituated for three days before polysomnographic recordings. The EEG/EMG recording cable was connected with a slip ring to enable mice to freely move. In optogenetic experiments, the fiber optic cable was connected with the implanted cannula, and another end of the optic fiber passed through the hole of the slip ring for attachment with a rotating optical joint (Doric Lenses, Canada). Cortical EEG and neck EEG signals were amplified, filtered (Biotex Kyoto, Japan), and digitized at a sampling rate of 512 Hz and were recorded with a Power 1401 digitizer and Spike2 software (CED, Cambridge, UK). The Spike2 data were converted to text format for SleepSign software (Kissei Comtec, Nagano, Japan). The polysomnographic signals were filtered (EEG: 0.5–30 Hz; EMG: 20–200 Hz) and automatically scored off-line by 4-s epochs of wakefulness, REM, and NREM sleep via SleepSign software (Kissei Comtec, Nagano, Japan) according to standard criteria.²⁷ As a final step, defined sleep–wake stages were examined visually and were corrected if necessary. Wakefulness was defined as desynchronized low-amplitude EEG activity and heightened EMG activity with phasic bursts. NREM sleep was defined as synchronized, high-amplitude, low-frequency (delta band: 0.5–4 Hz) EEG activity and low EMG activity compared with that of wakefulness (and without phasic bursts). REM sleep was defined as having a

pronounced theta rhythm (6–10 Hz) and low EMG activity. Power spectral density was estimated for EEG delta power using a short-time Fourier transform. We used a 2-s Hamming window and 95% overlap. For EMG amplitude analysis, the RMS of the EMG signal was calculated using a moving window (0.1-s span). The EEG delta power and EMG RMS were normalized to typical NREM sleep delta power and EMG RMS, respectively.

Photostimulation

After viral infections and cannulae/electrode implantations, mice recovered in individual housing for at least two weeks. Mice were connected to fiber-optic patch cords (Newdoon, China) with another side connected to optic rotary joints (1FC_2FC, Doric Lenses, Canada) to allow free movement. Another patch cord was connected from the joints to a 473-nm laser (BL473T3-100, SLOC, Shanghai, China). We adjusted the light power of the lasers such that the light power exiting each optic-fiber tip was 10 mW. Light pulse trains were controlled by the digital output function of a Power 1401 digitizer and were programmed by Spike2 software. In acute photostimulation experiments, we monitored EEG/EMG signals by Spike2 in real time in order to precisely time the delivery of optical stimuli after identifying stable NREM sleep epochs. The latency to wakefulness from NREM or REM sleep is defined as the time from the laser onset to the first appearance of wakefulness episode. The individual mouse latency to wakefulness was calculated by averaging all stimulation trials of corresponding individuals, and averaging all individual mouse latency as the final latency values.

Fiber photometry

After viral infection and implantations of cannulae and electrodes, mice were individually housed for at least two weeks for recovery from the surgery and expression of the virus. Fluorescent emission was recorded with a fiber photometry system (Thinkerbiotech, Nanjing, China) using methods similar to those of previous studies.^{16,47} Briefly, to record GCaMP fluorescence signals, the laser beam from a 488-nm laser (OBIS 488LS, Coherent, USA) was reflected by a dichroic mirror (MD498; Thorlabs), focused by a x 10 objective lens (NA=0.3, Olympus) and then coupled to an optical commutator (Doric Lenses, Canada). An optical fiber (230-mm O.D., NA=0.37, 1-m long) guided the light between the commutator and the implanted optical fiber. The laser power was adjusted at the tip of the optical fiber to a low level of 10–20 μ W to minimize bleaching. The GCaMP fluorescence was bandpass filtered (MF525-39, Thorlabs) and collected by a photomultiplier tube (R3896, Hamamatsu). To record RCaMP fluorescence signals, the 580 nm LED was used. RCaMP fluorescence was band pass filtered (MF615-20). An amplifier (C7319, Hamamatsu) was used to convert the photomultiplier-tube current output to voltage signals, which was further filtered through a low-pass filter (40-Hz cut-off; Brownlee 440). The analogue voltage signals were digitalized at 512 Hz and recorded by a Power 1401 digitizer and Spike2 software (CED, Cambridge, UK).

Chemicals and drug administrations

The CNO (Cat NO: C4759, LKT, USA) was dissolved in saline and intraperitoneally (i.p.) injected in mice. For control groups, mice were injected with saline only.

Auditory tone test

To examine whether striatal D₁R neurons response to external stimuli, high-frequency auditory tonal stimuli (70 dB, 2–4 kHz, 5-s duration) were applied during NREM sleep or wakefulness periods, as previous described.^{46,48} The speaker was placed at the top of the cage, about 50 cm away from the mouse. The auditory tone intensity inside the cage was calibrated with a sound meter (Uni-Trend UT350, Dongguan, China). The speaker was controlled by the digital output function of a Power 1401 digitizer and was programmed by Spike2 software.

Electric footshocks

Animals were introduced into an acrylic box (16 x 16 x 30, L x W x H in cm) with a metal grid floor. Mice were allowed to explore and habituate to the operant box for 10 min. Mild footshocks (0.35 mA, 3 s) were delivered by an isolator (Nihon Kohden, Japan). TTL pulses were sent to the Power 1401 digitizer for accurate time stamping.

Air puffs

Animals were introduced into an acrylic cage and allowed to explore and habituate for 10 min. Brief air puffs were delivered by a compressed air duster (Sunto, Shanghai, China). Each time stamp was added by the keyboard function of Spike2.

Histology

Mice were deeply anaesthetized with an overdose of sodium pentobarbital and were transcardially perfused with PBS, followed by 4% paraformaldehyde in PBS. Brains were extracted and post-fixed with 4% paraformaldehyde at 4°C overnight and were then cryoprotected in 30% sucrose with PBS until they sank to the bottom of tube. The brains were embedded in OCT and were sectioned on a freezing microtome (30- μ m sections), collected in PBS, and stored at 4°C. Sections underwent immunohistochemical staining as described below. Sections were washed in 0.1 M of PBS and were then incubated in a primary antibody (rabbit anti-tyrosine hydroxylase, Cat#: AB152, 1:3000, Millipore, USA) overnight at room temperature. On the second day, the sections were washed in PBS and incubated in secondary antibody (Alexa Fluor 488 donkey anti-rabbit, Cat#: 711-545-152, 1:1000, Jackson ImmunoResearch, USA)

for 2 h at room temperature. Sections were washed in PBS and then mounted onto glass slides and coverslipped with a mounting medium (Southern Biotech). YFP, mCherry, and GCaMP6f were directly detected by their native fluorescent signals, so no antibody was used for detecting these fluorescent proteins, as previous reported.¹³ Before mounted, slices were counterstain with DAPI. For mCherry staining, the primary antibody (rabbit anti-mCherry, Cat#: 632496, Clontech) was used at a 1:3000 dilution and incubated on a shaker plate overnight at room temperature. The secondary antibody (Biotinylated Donkey anti-rabbit, Cat#: 711-065-152, Jackson ImmunoResearch) was incubated at a 1:1000 dilution for 2 h on a shaker plate at room temperature. Tissue sections were then incubated with Avidin-Biotin Complex (Vectastain ABC HRP kit, Cat#: PK-6100, Vector Laboratories, USA) at a 1:1000 dilution for 1 h, and immunoreactive cells were produces a brown reaction with DAB substrate kit (Vector DAB Peroxidase Substrate, Cat#: SK-4100, Vector Laboratories, USA). Non-confocal images were captured by a fluorescent microscope (IX71 and VS120, Olympus). High-resolution fluorescent images were collected on a confocal microscope (FV-1000, Olympus). Digital images were processed using FV-1000 Viewer 2.0 and Adobe Photoshop CS6 software to minimally adjust brightness and contrast.

QUANTIFICATION AND STATISTICAL ANALYSIS

Sample sizes were determined based on previous studies that used optogenetics and fiber photometry for investigating neural circuits underlying sleep-wake state regulation.^{16,49} Data are presented as the mean \pm standard error of the mean (s.e.m.) unless otherwise indicated. Paired and unpaired t-tests were used for comparisons between the two groups. One-way analyses of variance (ANOVAs) were used to compare more than two groups. Two-way ANOVAs were used to perform group comparisons with multiple measurements. All statistical tests were two-tailed. Data were considered to be statistically significant at $p < 0.05$. We analyzed all data using Prism 7.0 (GraphPad Software) and MATLAB R2016a software.

For the analysis of optogenetic data, the 95% confidence interval (CI) for brain-state probabilities was estimated using a bootstrap procedure, similar to the procedure reported in a previous study.⁵⁰ For an experimental group of “n” mice, with mouse “i” comprising “mi” trials, we calculated the CI as follows: first, we calculated the brain-state probabilities of mouse “i” with “mi” trials. Then, we recalculated the mean probabilities across the “n” mice by 100,000 iterations of random sampling with replacement. The lower and upper CIs were then extracted from the distribution of the resampled mean values.

Photometry data analysis was performed with customized MATLAB software. The photometry data were exported in the MATLAB Mat format from Spike2 software for further analysis. The signal data were smoothed with a moving-average filter (0.2-s span). For each experiment, the photometry signal, F , was converted to $\Delta F/F$ by calculating $\Delta F/F = (F - F_{\text{mean}})/F_{\text{mean}}$, where F_{mean} is the average of the recording episode. For the sleep–wake analysis, we recorded data for about 4–6 h per mouse, and calculated the averaged $\Delta F/F$ during all times of wakefulness, NREM-sleep, and REM-sleep states. For state-transition analyses, we identified each state transition and aligned $\Delta F/F$ with a ± 50 s window before and after the switch point. For [Figure S5](#), each mouse was calculated by 8 sessions per stage, F_{peak} is the average value of total peaks in each session, $F_{\text{frequency}}$ is the average of the peak number in each session. For behavioral analysis, the photometry signal, F , was converted to $\Delta F/F$ by calculating $\Delta F/F = (F - F_0)/F_0$, where F_0 was the baseline signal.